JACS
JOURNAL OF THE AMERICAN CHEMICAL SOCIETY

pubs.acs.org/JACS
Article

Organophosphonate Ligation Approach for the Controlled Assembly of Gigantic Polyoxometalate Clusters

Mengyuan Cheng, Yujia Li, Rongqing Tang, Yubin Ma, De-Liang Long,* Leroy Cronin,* and Weimin Xuan*

Cite This: J. Am. Chem. Soc. 2026, 148, 12890−12897

Read Online

ACCESS | Metrics & More | Article Recommendations | Supporting Information

ABSTRACT: The controlled assembly of gigantic polyoxometalate (POM) clusters remains one of the most formidable challenges in molecular self-assembly, as it is highly dependent on delicate synthesis parameters that can yield a wide variety of products. In this study, we report the synthesis of a series of unprecedented wheel-shaped molybdenum-blue (MB) clusters directed by organophosphonate (L) and acetate ligands, resulting in a new range of giant MB-type POMs: $\{Mo_{136}Na_4\}$, $\{Mo_{120}\}$, $\{Mo_{118}Na_2\}$, $\{Mo_{118}\}$, and $\{Mo_{157}\}$. These structures, constructed from fundamental $\{Mo_1\}$, $\{Mo_2\}$, and $\{Mo_8\}$ building blocks, exhibit new features of organic ligand coordination on their exterior surfaces. Notably, the $\{Mo_{157}\}$ framework acts as a host capable of capturing the fully reduced ε-Keggin-based $\{Mo_{16}\}$ guest. It represents the first pure dodecameric Mo wheel reported to date. Systematic variation of reaction parameters—including ligand type, concentration, solvent composition, and precursor identity—enabled precise control over cluster topology, revealing competitive coordination between organophosphonate and acetate ligands. Structural analyses unveiled new connection modes involving reduced edge-sharing $\{e\text{-}Mo_2\}$ units and their derivative $\{Mo_3L_2\}$ motifs, which reinforce the overall cage architecture. Mass spectrometry and NMR spectroscopy confirmed the structural integrity of these assemblies in solution. This work not only expands the library of gigantic MB clusters but also establishes a new strategy for their controlled construction using anchored organophosphonate ligands. The resulting clusters exhibit significantly enhanced solubility in organic solvents compared with traditional MB species, offering new opportunities for postsynthetic modification, improved interactions with biomolecules, and diverse applications.

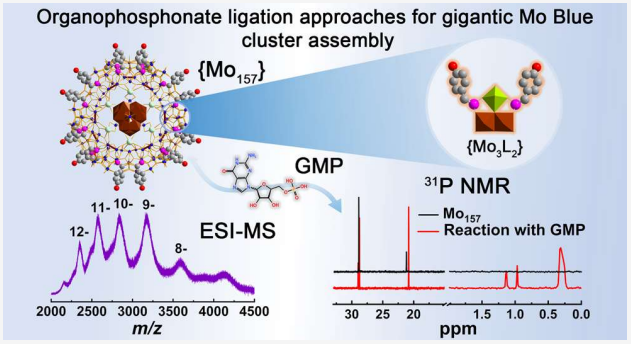

INTRODUCTION

Polyoxometalates (POMs) are a unique class of discrete metal-oxo clusters known for their diverse structures and rich physicochemical properties.[1,2] Gigantic polyoxomolybdate (POMo) clusters represent an important subclass of POMs, consisting of hundreds of molybdenum centers, and hold great potential for applications in catalysis,[3,4] sensing,[5] materials,[6] and biomedicine.[7] Based on their degree of reduction and structural building blocks, gigantic POMo clusters are conventionally classified into three types, namely, molybdenum blues (MBs), molybdenum browns (Mo browns), and molybdenum reds (Mo reds), which together give rise to a wide variety of fascinating structures.[8−10] MBs' blue coloration is due to the delocalization of their reducing electrons, while the color displayed by Mo browns and Mo reds comes from localized reducing electrons on the edge-sharing $\{e\text{-}Mo_2\}$ units.[8a] Structurally, MBs and Mo browns share common pentagonal $\{Mo_6\}$ building units, while Mo browns and Mo reds both incorporate reduced $\{e\text{-}Mo_2\}$ motifs. To date, a variety of remarkable architectures have been successfully designed and synthesized, including the wheel-shaped $\{Mo_{154}\}$[8c] and $\{Mo_{176}\}$[11] MB, the Keplerate-type K-$\{Mo_{132}\}$[12] Mo brown, and the cage-like $\{Mo_{240}\}$[9c] Mo red. While these achievements mark a significant breakthrough in POM chemistry, precise control over cluster size, topology, and composition through rational modulation of reduction degree, pH, and ligand coordination remains in the exploratory stage.[13] Further understanding of the self-assembly mechanism and the roles of various structure-directing agents is essential for enabling the predictable and controllable synthesis of novel gigantic POMo clusters.

Within the MB family, assembled under acidic and reductive conditions, clusters are particularly fascinating due to their

Received: December 1, 2025
Revised: March 2, 2026
Accepted: March 5, 2026
Published: March 17, 2026

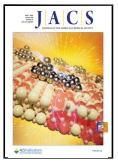

https://doi.org/10.1021/jacs.5c21427
J. Am. Chem. Soc. 2026, 148, 12890−12897

dynamic self-assembly behaviors and aesthetically complex architectures. MB wheel clusters are constructed from basic building blocks (BBs), including pentagon-based $\{Mo_8\}$, corner-sharing $\{c\text{-}Mo_2\}$, and supporting $\{s\text{-}Mo_1\}$ units, which are connected in a defined manner to form wheel structures. Generally, the wheel sizes are controlled by the number and type of linker $\{Mo_2\}$ units that connect $\{Mo_8\}$ BBs (Scheme 1).[14,15] For example, the number of $\{c\text{-}Mo_2\}$ units decreases

Scheme 1. Transformation of $\{Mo_2\}$ Linker Units from $\{c\text{-}Mo_2\}$ to $\{e\text{-}Mo_2\}$ and Derived $\{Mo_3L_2\}$ Leading to Structural Evolution of Gigantic POMo Clusters, Revealing the Importance of Building Blocks in Structural Assembly[a]

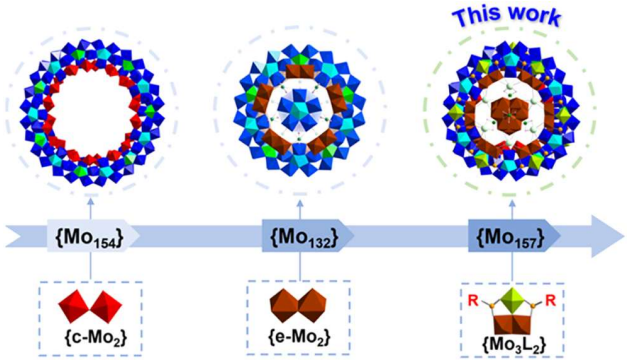

[a]L represents organophosphonate ligands.

from 16 to 14 as the structure changes from hexadecamer $\{Mo_{176}\}$[11] to tetradecamer $\{Mo_{154}\}$.[8c] Recent studies have demonstrated that the $\{c\text{-}Mo_2\}$ units can be replaced with smaller, reduced edge-sharing $\{e\text{-}Mo_2\}$ units, leading to the formation of decameric capped C-$\{Mo_{132}\}$[16] and lantern-shaped L-$\{Mo_{132}\}$[17] (Scheme 1). The $\{e\text{-}Mo_2\}$ is relatively reactive, with its surface-coordinated water molecules readily exchangeable for various ligands, such as sulfate, phosphate, and carboxylate.[18] We hypothesized that ligand variation on the $\{e\text{-}Mo_2\}$ unit can create new interaction sites, fascinating the generation of new BBs. Therefore, precise modulation of the number and even structural evolution of $\{e\text{-}Mo_2\}$ units is very important for the development of novel gigantic MB clusters (Scheme 1).

Organophosphonates are versatile ligands for cluster synthesis due to their diverse coordination modes, intermediate ligand field strength, and tunable steric properties.[19] However, their application in the construction of POMo clusters remains relatively limited.[20,21] Most reported examples involve low-nuclearity frameworks containing one or a few phosphonate groups. Representative POMo structures include $[(Mo_2{}^{V}O_4)_4(O_3PCH_2PO_3)_4(CO_3)_2]^{12-}$,[21a] $[Na(SO_3)_2(C_6H_5PO_3)_4Mo_4{}^{V}Mo_{14}{}^{VI}O_{49}]^{5-}$,[21b] and $[Mo_5{}^{V}Mo_7{}^{VI}O_{30}(BPO_4)_2(C_6H_5O_3P)_6]^{5-}$.[21d] Recent studies have shown that phenylphosphonate ligands can actually replace sulfate or sulfite groups and functionalize the inner surface of gigantic POMo clusters by linking with well-established BBs.[22] This implies that organophosphonates have the potential to promote the formation of robust coordinate bonds suitable for the assembly of high-nuclearity clusters. Given the abundance of reactive synthons in highly reducing aqueous solutions, we propose that organophosphonates may also interact with $\{e\text{-}Mo_2\}$ units, thereby triggering the generation of new building blocks. Rational integration of these newly generated and existing BBs will thereby lead to the construction of novel gigantic assemblies with emergent structural and functional properties (Scheme 1).

Herein, we report five novel MB clusters where organophosphonate ligands (L) induce the formation of $\{e\text{-}Mo_2\}$-based $\{Mo_3L_2\}$ units: $\{Mo_{136}Na_4L_{18}\}$ (**1**), $\{Mo_{120}L_{12}\}$ (**2**), $\{Mo_{118}Na_2L_{20}\}$ (**3**), $\{Mo_{118}L_{16}\}$ (**4**), and $\{Mo_{157}L_{18}\}$ (**5**) (Figure 1 and Figures S2–S4). Compounds **1**–**4** possess a decameric wheel framework built from pentagon-based $\{Mo_8\}$, $\{Mo_1\}$, and $\{Mo_3L_2\}$ (incorporating variant $\{Mo_2NaL_2\}$) units. In contrast, compound **5** forms a dodecameric wheel assembled from $\{Mo_8\}$, $\{Mo_1\}$, $\{Mo_3L_2\}$, and $\{c\text{-}Mo_2\}$ linkers, with a central fully reduced ε-Keggin $\{Mo_{12}{}^{V}\}$-based $\{Mo_{16}\}$ guest encapsulated within the hollow interior (Figure 1e). In particular, the $\{Mo_3L_2\}$ BB consists of an $\{e\text{-}Mo_2\}$ dimer augmented by a growing $\{g\text{-}Mo_1\}$ unit joined by two organophosphonate ligands. Structural analyses unveil a series of new connection modes involving $\{e\text{-}Mo_2\}$ and $\{Mo_3L_2\}$ units, which reinforce the overall structural architecture. Mass spectrometry and NMR spectroscopy confirm the structural integrity of these assemblies in solution. These compounds have been comprehensively characterized as detailed in the Supporting Information (Figures S13–17, Tables S4 and S5) with formulas:

$$(NH_4)_{40}H_{16}[H_{10}Mo_{136}Na_4(H_2O)_{16}O_{390}(CH_3COO)_{10}(PO_3C_7H_7)_{18}]\cdot ca.210H_2O\cdot(CH_3COOH)_7\ \mathbf{1}$$
$$\equiv (NH_4)_{40}H_{16}\{\mathbf{1a}\}\cdot ca.210H_2O\cdot(CH_3COOH)_7$$

$$(NH_4)_{20}H_{22}[H_{10}Mo_{120}(H_2O)_{19}O_{344}(CH_3COO)_8(PO_3C_7H_7)_{12}]\cdot ca.130H_2O\ \mathbf{2}$$
$$\equiv (NH_4)_{20}H_{22}\{\mathbf{2a}\}\cdot ca.130H_2O$$

$$(NH_4)_{24}H_{12}[H_{10}Mo_{118}Na_2(H_2O)_{18}O_{338}(PO_3C_7H_6OCH_3)_{20}]\cdot ca.155H_2O\cdot(CH_3COOH)_{10}\ \mathbf{3}$$
$$\equiv (NH_4)_{24}H_{12}\{\mathbf{3a}\}\cdot ca.155H_2O\cdot(CH_3COOH)_{10}$$

$$(NH_4)_{24}H_6[H_{10}Mo_{118}(H_2O)_{18}O_{336}(CH_3COO)_4(PO_3C_7H_6OCH_3)_{16}]\cdot ca.130H_2O\ \mathbf{4}$$
$$\equiv (NH_4)_{24}H_6\{\mathbf{4a}\}\cdot ca.130H_2O$$

$$K_{27}Na_5H_4[H_{24}Mo_{157}(H_2O)_{35}O_{456}(PO_3C_7H_6OH)_{18}]\cdot ca.240H_2O\ \mathbf{5}$$
$$\equiv K_{27}Na_5H_4\{\mathbf{5a}\}\cdot ca.240H_2O$$

RESULTS AND DISCUSSION

Compound **1** was successfully synthesized via the hydrothermal reaction of an aqueous mixture of $(NH_4)_6Mo_7O_{24}\cdot 4H_2O$ (0.4 mmol), $N_2H_4\cdot 2HCl$ (0.5 mmol), benzylphosphonic acid (0.4 mmol), CH_3COONa (0.5 mmol), 1 mL of acetic acid, and a small amount of HCl in a capped vial at 120 °C for 3 days, which generally favored the formation of the desired framework (Figure S1). Under these highly reducing conditions, the formation of a cyclic cluster with a high Mo(V)/Mo(total) ratio is promoted. Meanwhile, the strong coordination of the organophosphonate to $\{e\text{-}Mo_2{}^{V}\}$ unit not

https://doi.org/10.1021/jacs.5c21427
J. Am. Chem. Soc. 2026, 148, 12890−12897

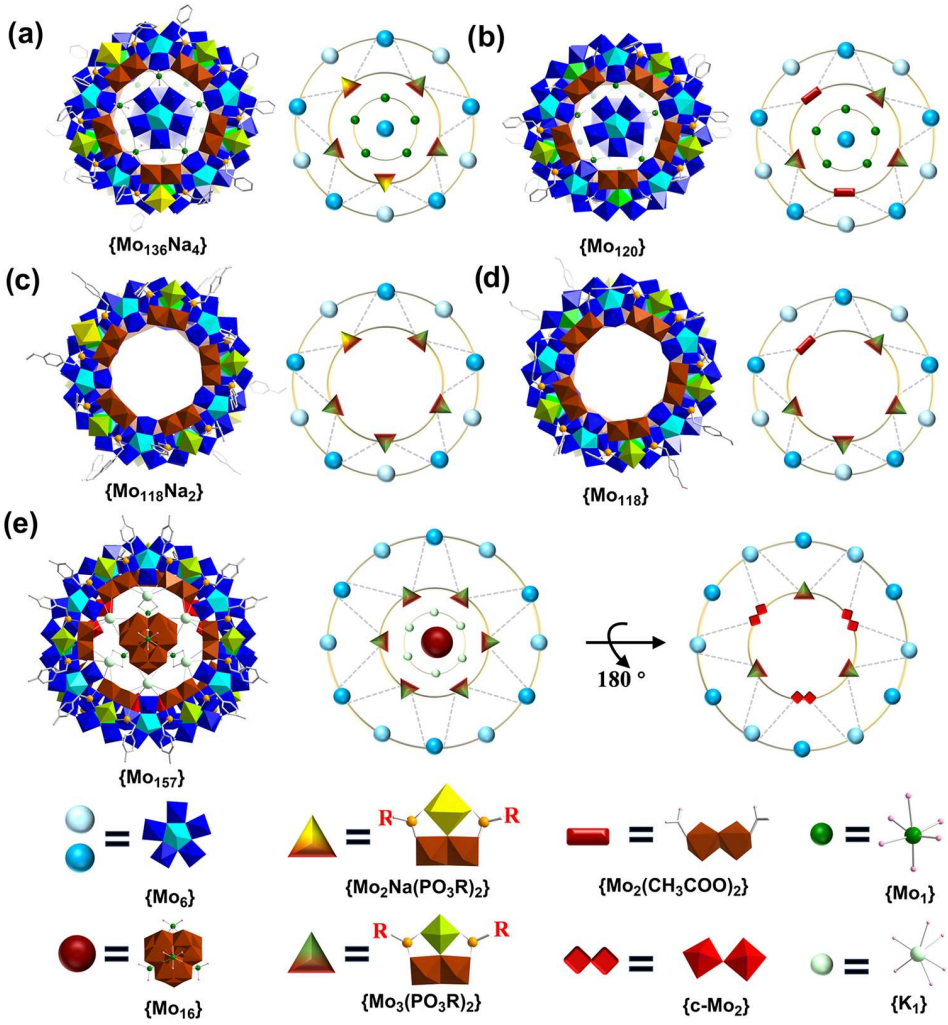

Figure 1. Structural evolution of MB wheels directed by different ligand systems. (a–e) View of the molecular structure of **1a–5a** (left) and corresponding simplified connection models (right) with building units defined at the bottom. {s-Mo_1}, bright green polyhedron; {e-Mo_2}, brown polyhedron; {c-Mo_2}, red polyhedron; {Mo_6}, blue polyhedron pentagonal units with cyan polyhedron center; {g-Mo_1}, lime polyhedron; {Mo_1} linker, green ball; K, light green ball; Na, yellow polyhedron; O, rose ball; C, gray ball; and P, light orange ball. Bottom: simplified schematic symbols used in the connection models and their represented structural building blocks ({Mo_{16}}, {Mo_2}, {Mo_6}, {Mo_3}, etc.).

only stabilizes this fully reduced species but also triggers the generation of the {Mo_3L_2} motif. The synergistic interplay of these two critical factors facilitates the assembly of the giant Mo-blue wheel during ligand functionalization. Compounds **2–5** were formed by varying the amounts of ligands, acid content (pH value), and source of molybdates under similar conditions. The dominant factor lies in alteration of the type of organophosphonates, resulting in benzyphosphonate-functionalized close-shell **1** and **2**, methoxybenzyl phosphonate-functionalized open-shell **3** and **4**, as well as hydroxybenzyl phosphonate-functionalized **5** featuring a cluster@cluster architecture. Moreover, the cation also plays an important role, as **5** can only be obtained when a potassium ion is adopted for the assembly.

Single-crystal X-ray structural analysis reveals that **1** crystallizes in the monoclinic system with centrosymmetric space group *C*2/*m* (Table S1), exhibiting a remarkable closed-shell ellipsoidal architecture (Figure 1a). As depicted in Figure 2, ellipsoidal cluster {Mo_{136}} **1a** is assembled from multiple pentagon-based {Mo_8} and various bridging/supporting units. It is organized into two centrosymmetrically related hemispheres of a {Mo_{63}}-type configuration. Each {Mo_{63}} hemisphere is composed of a {Mo_{52}} ring and an additional pentagon-centered {Mo_{11}} capping fragment. The {Mo_{52}} ring is built from three {Mo_3}, two {Mo_2Na}, and five {Mo_8} units. The {e-Mo_2} components from the three {Mo_3} and two {Mo_2Na} units are positioned along the rim of the {Mo_{52}} inner ring and are referred to as rim-{e-Mo_2} units (Figure S7). Additionally, five other {e-Mo_2} units are formed between the {Mo_{52}} ring and the {Mo_{11}} capping fragment. Each of these beam-{e-Mo_2} units comprises one Mo atom from the pentagon apex of a {Mo_8} unit on the {Mo_{52}} ring and a Mo atom from the {Mo_{11}} cap. These beam-{e-Mo_2} units function as structural "beams", extending outward from the main body of the {Mo_{52}} ring to support the {Mo_{11}} cap. The rim-{e-Mo_2} units feature a Mo···Mo distance of ca. 2.55 Å, significantly shorter than that in the corner-sharing counterparts {c-Mo_2} observed in conventional MB wheels, leading to a more compact wheel diameter. The beam-{e-Mo_2} has a Mo···Mo distance of ca. 2.62 Å, effectively bridging the {Mo_{52}} ring and the {Mo_{11}} cap. Due to the structural differences between the {Mo_3} and {Mo_2Na} units, the {Mo_{63}}

https://doi.org/10.1021/jacs.5c21427
J. Am. Chem. Soc. 2026, 148, 12890–12897

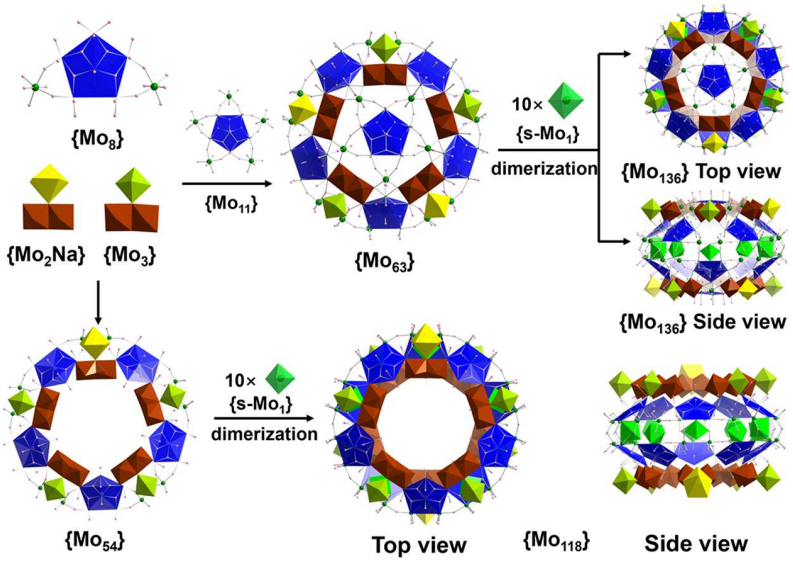

Figure 2. Schematic representation of the construction of $\{Mo_{136}\}$ **1a** and $\{Mo_{118}\}$ **3a** from the pentagon-based $\{Mo_8\}$, $\{Mo_2Na\}$, and $\{Mo_3\}$ building blocks with the aid of the supporting units $\{s\text{-}Mo_1\}$. The $\{Mo_{63}\}$ features a central ring capped by a $\{Mo_{11}\}$ moiety. The color scheme is the same as that in Figure 1. Organic ligands are omitted for clarity.

hemisphere deviates from ideal C_{5v} symmetry and instead adopts C_s symmetry, with two distinguishable head and tail ends. Two such $\{Mo_{63}\}$ hemispheres are joined in a head-to-tail fashion via 10 $\{s\text{-}Mo_1\}$ supporting units inside the ellipsoid equator, resembling the structural motif observed in C-$\{Mo_{132}\}$.[16]

In MB wheel systems, ligands readily replace the coordinated water molecules located on the inner surface of $\{c\text{-}Mo_2\}$ units,[23] thereby enabling effective stabilization and functionalization of the framework. In **1a**, both bidentate acetate and tridentate phosphonate ligands substitute the water ligands bound to Mo sites on the $\{e\text{-}Mo_2\}$ unit, distributing over the inner and outer surfaces of the wheel. Specifically, ten acetate ligands are attached to the beam-$\{e\text{-}Mo_2\}$ units from the inner side, while tridentate organophosphonate ligands bind to the rim-$\{e\text{-}Mo_2\}$ units (Figure S8). The latter further capture either an additional Mo atom, giving rise to a novel $\{Mo_3L_2\}$ building block, or a Na atom, resulting in a $\{Mo_2Na\}$ unit (Figure S9). Through bidentate and tridentate coordination modes, acetate and organophosphonate ligands serve as "molecular nails," reinforcing the rigidity of the entire cage-like architecture. The incorporation of edge-sharing $\{e\text{-}Mo_2\}$ units and their derivatives $\{Mo_3\}$ and $\{Mo_2Na\}$ not only tighten the framework but also differentiates it from previously reported systems employing corner-sharing $\{c\text{-}Mo_2\}$ linkers. This introduces a new structural motif for designing high-nuclearity molybdenum-oxide clusters with tunable internal cavities. Moreover, the incorporation of organophosphonate ligands significantly improves the solubility of these clusters in a variety of organic solvents (Figure S25), opening avenues for postsynthetic modification and enhanced compatibility with functional materials.

2 crystallizes in the monoclinic space group *C*2/*m* (Table S1). Unlike **1a**, **2a** $\{Mo_{120}\}$ displays a markedly reduced incorporation of the $\{Mo_{11}\}$ capping unit with an occupancy of ~ 0.2. Moreover, the higher concentration of acetic acid used in the synthesis of **2a** induces a competitive ligand substitution, whereby acetate ligands replace the phosphonate groups at the corresponding $\{Mo_2Na\}$ sites in **1a**. This transformation yields $\{Mo_2(CH_3CO_2)_2\}$ units and eliminates the involvement of Na (Figure 1b). These observations reveal that subtle variations in acetic acid concentration not only influence the incorporation of large building blocks but also govern the competitive coordination dynamics between acetate and organophosphonate ligands. Such modulation enables fine-tuning of the final cluster architecture and enhances the structural stability.

3 and **4** crystallize in the monoclinic space group $P2_1/n$ and *C*2/*m*, respectively (Table S2). **3a** and **4a** adopt a decameric wheel structure composed of two $\{Mo_{54}\}$ hemispheres joined by 10 $\{s\text{-}Mo_1\}$ units. The $\{Mo_{54}\}$ hemisphere in **3a** is built from four $\{Mo_3\}$, one $\{Mo_2Na\}$, and five $\{Mo_8\}$ units (Figure 2). The structural difference between **3a** and **4a** resembles that observed between **1a** and **2a**: upon increasing the amount of acetic acid in the reaction mixture, acetate ligands replace the phosphonate groups bound to the $\{Mo_2Na\}$ units, resulting in the formation of the $\{Mo_2(CH_3CO_2)_2\}$ unit in **4a** (Figure 1c,d). As a result, **4a** represents the acetate-substituted analogue of **3a**, once again highlighting the competitive coordination between the acetate and organophosphonate ligands at the $\{Mo_2Na\}$ sites.

Following systematic optimization of the synthetic conditions, compound **5** was successfully obtained in a good yield. Single-crystal X-ray structural analysis reveals that it crystallizes in the monoclinic space group *P*2/*n* (Table S3). The structure of **5a** can be described as a dodecameric wheel composed of two nonequivalent hemispherical shells, top $\{Mo_{82}\}$ and bottom $\{Mo_{63}\}$, joined by 12 $\{s\text{-}Mo_1\}$ supporting units, each located behind a pentagonal unit inside the equatorial backbone (Figures 3 and S4), thereby constructing the first pure dodecameric Mo wheel reported to date. The top $\{Mo_{82}\}$ hemisphere is constructed from six $\{Mo_8\}$ and six $\{Mo_3\}$ building blocks arranged alternately to delineate an elliptical cavity that encapsulates a central ε-Keggin-based $\{Mo_{16}\}$ guest (Figure S10). This $\{Mo_{16}\}$ guest is composed of a fully reduced ε-Keggin core $\{Mo_{12}^{V}\}$ and four $\{Mo^{VI}\}$ add-on units and represents the first instance of such a guest being captured in MB synthesis. Several potassium ions are also located between the $\{Mo_{16}\}$ guest and the surrounding wheel

https://doi.org/10.1021/jacs.5c21427
J. Am. Chem. Soc. 2026, 148, 12890−12897

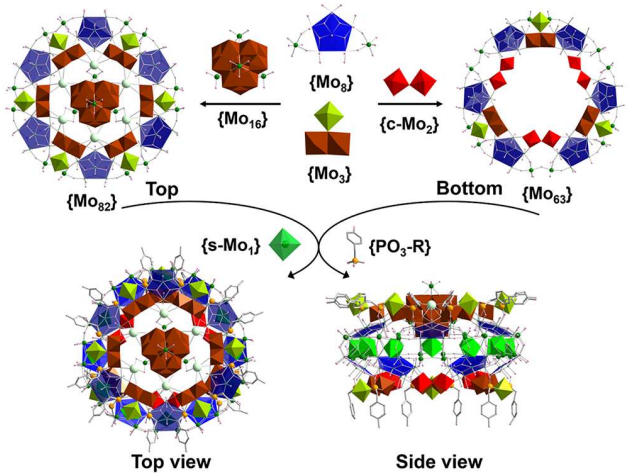

Figure 3. Schematic representation of the construction of $\{Mo_{157}\}$ **5a** from the pentagon-based $\{Mo_8\}$ and $\{Mo_3\}$ building blocks with the aid of the bridging units $\{c\text{-}Mo_2\}$, where the top $\{Mo_{82}\}$ unit encapsulates a central ε-Keggin-based $\{Mo_{16}\}$ guest and connects to the bottom $\{Mo_{63}\}$ through 12 $\{s\text{-}Mo_1\}$ linkers along the equatorial backbone. The color scheme is the same as Figure 1.

framework. Their ionic radius matches the cavity of the dodecameric wheel remarkably well, allowing them to serve a dual role: they not only provide structural reinforcement for the host framework but also anchor the encapsulated $\{Mo_{16}\}$ guest by acting as electrostatic linkers between the host and the guest. In contrast, the bottom $\{Mo_{63}\}$ hemisphere, although also constructed from six $\{Mo_8\}$ units, features a distinct linkage pattern in which three $\{Mo_3\}$ and three $\{c\text{-}Mo_2\}$ units are alternatively arranged along the inner rim of the ring (Figure 4). This structural asymmetry between the two

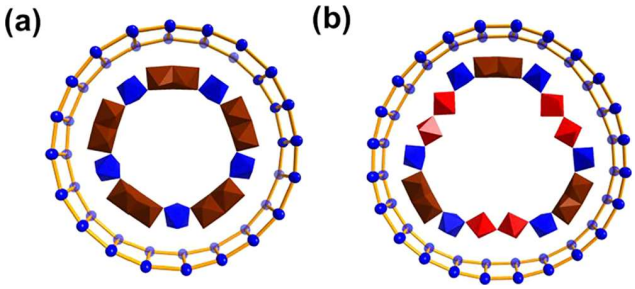

Figure 4. (a) Schematic representation of **4a** and **5a** by connecting Mo atoms on the rim and equator of the wheels. $\{e\text{-}Mo_2\}$ and $\{c\text{-}Mo_2\}$ units on the inner rim are highlighted in dark red and red polyhedra.

hemispheres is a defining characteristic, giving rise to the unique elliptical wheel architecture of $\{Mo_{157}\}$. The organophosphates on two adjacent $\{Mo_{157}\}$ clusters are interconnected by $\pi-\pi$ stacking (centroid-to-centroid distance of approximately 3.9 Å) to form a dimer (Figure S11). Consistent with **1a**–**4a**, 18 benzylphosphonate ligands were found on the exterior surface of **5a**, bridging the $\{Mo_6\}$ pentagons and $\{Mo_3\}$ units to reinforce the overall wheel structure.

Compared to traditional MBs, new clusters bearing organophosphonate ligands show greatly improved solubility in polar organic solvents including isopropanol, acetonitrile, and N,N-dimethylformamide, though they remain largely insoluble in dichloromethane (Figure S25 and Table S6). This gives rise to the opportunity to carry out mass spectrum analysis directly in organic media. Electrospray ionization-mass spectrometry (ESI-MS) was employed to study the solution behavior of compounds **4** and **5**. Despite the broad peak envelopes observed in the spectra, a common phenomenon in ESI-MS of giant POMs caused by association of counterions and solvent molecules,[24] the intact molecular species of **4a** based on the cluster $\{Mo_{118}O_{354}H_{46}(CH_3COO)_4(PO_3C_7H_6OCH_3)_{16}\}$ were clearly detected at charge states ranging from −7 to −10 (Table S7). These signals arise from adding different numbers of ammonium counterions and associated water molecules (Figures 5 and S26). Similarly, for **5**, all major peaks in the

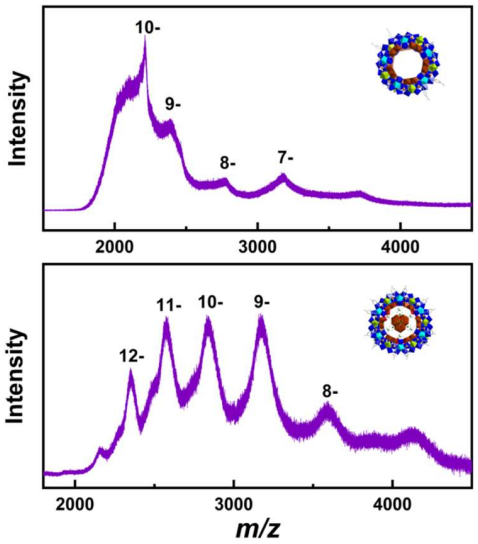

Figure 5. ESI-MS spectra of **4** and **5** in a CH_3CN solution.

spectrum could be assigned to species based on the cluster formula $\{Mo_{157}O_{456}H_{24}(H_2O)_{35}(PO_3C_7H_8OH)_{18}\}$ (Tables S8), with charge states ranging from −8 to −12 (Figures 5 and S27). These findings confirm the presence and stability of **4** and **5** in solution.

To gain detailed insight into the local environment of the phosphorus center within the compound, we examined the ^{31}P NMR spectrum of compound **5**. The spectrum (Figure 6) exhibits two distinct resonances at δ = 21.2 and 28.9 ppm with an intensity ratio of approximately 1:2. This contrasts with the single resonance observed for the free ligand at δ = 25.45 ppm, indicating that the phosphonate ligands experience two chemically nonequivalent environments upon incorporation into the cluster framework. Structurally, the phosphorus atom in the $-PO_3CH_2C_6H_4OH$ ligand is bonded to three oxygen atoms in an approximately trigonal geometry. These oxygen atoms, however, coordinate to three Mo centers with different oxidation states (two Mo^{VI} and one Mo^{V}, Figure 6b). This electronic and structural asymmetry leads to the formation of three conformational isomers of the $-PO_3CH_2C_6H_4OH$ ligand, arising from rotation around the P–C single bond. These isomers correspond to the 4-hydroxyphenyl (PhOH) group occupying either a trans (1 case) or cis (2 cases) orientation relative to the unique $O-Mo^{V}$ site (Figure 6b), consistent with the observed 1:2 resonance ratio in the NMR spectrum. In the crystal structure, it was found that the trans conformation positions the PhOH group perpendicular to the cluster's main axis, whereas the cis conformation aligns the

https://doi.org/10.1021/jacs.5c21427
J. Am. Chem. Soc. 2026, 148, 12890–12897

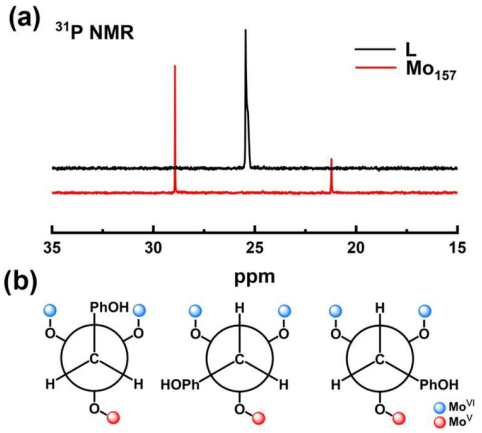

Figure 6. (a) ^{31}P NMR spectra of $\{Mo_{157}\}$ and hydroxybenzyl phosphonic acid in D_2O. (b) Schematic representation of the three possible conformational isomers of the benzylphosphonate ligand arising from rotation around the P−C single bond. The $-PO_3$ group is bound to three Mo centers, including two Mo^{VI} (blue) and one Mo^{V} (red). These isomers correspond to the 4-hydroxyphenyl (PhOH) group occupying either a trans (the first case) or cis (the latter two cases) orientation relative to the unique O−Mo^{V} site.

PhOH group parallel to the axis (Figure S12). In the solid state, the crystal packing force arising from supramolecular interactions may overcome the energy barrier between these conformational isomers, favoring one dominant orientation. This is exemplified in the crystal structure of $\{Mo_{157}\}$, where all PhOH groups are oriented parallel to the main axis at one end of the cluster and all perpendicular at the other (Figure S12). In solution, however, it is believed that the three conformational isomers coexist with equal probability, resulting in a theoretical 1:2 ratio as observed.

Given the presence of three sets of $\{c\text{-}Mo_2\}$ units in $\{Mo_{157}\}$ and the known lability of the two coordinated water molecules at the $\{Mo_2\}$ sites, we hypothesized that a third type of comparable ligand such as phosphate could substitute at these positions. To explore the potential of postsynthetic modification of the cluster's exterior microenvironment and test the interaction with biomolecules, we conducted a ligand substitution reaction using guanosine monophosphate (GMP) as a model system (Figure 7). When **5a** was mixed with GMP in D_2O for 1 h at ambient temperature, the ^{31}P NMR spectrum revealed splitting of original organophosphonate peak at 28.9 ppm into two distinct signals at δ 28.98 and 28.76 ppm. Concurrently, the signal at δ 20.81 ppm (originally 21.2 ppm) increased in relative intensity. At the same time, new phosphate resonances appeared at δ 0.96 and 1.12 ppm, characteristic of monoester phosphate environments derived from GMP. These are distinct from the signal at δ 0.31 ppm, which is assigned to free GMP.[25] Collectively, these spectral changes support the occurrence of ligand substitution at cluster sites adjacent to the bound organophosphonate groups. The ^{31}P NMR data confirm that nucleotides such as GMP can successfully replace surface-coordinated water molecules, enabling controlled functionalization of the MB cluster. The resulting Mo−O−PO_3−nucleotide linkage provides clear spectral markers and establishes a practical starting point for subsequent probe reactions, including simple site-selective labeling strategies.

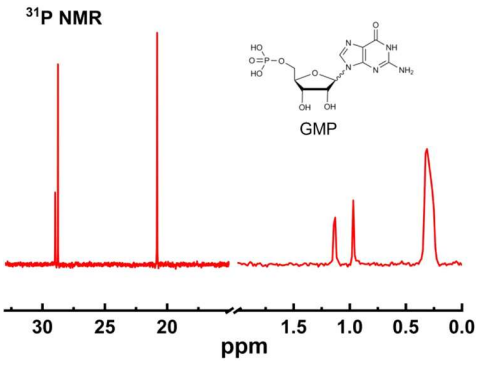

Figure 7. ^{31}P NMR spectrum of the solution after GMP ligand reacts with $\{Mo_{157}\}$, showing two new signals around 1.0 ppm, corresponding to coordinated phosphate sites of GMP on the cluster.

CONCLUSION

In summary, we have successfully achieved the controlled assembly of five novel molybdenum-blue wheel clusters through the use of semirigid organophosphonate ligands. This study demonstrates that subtle changes in ligand identity and reaction conditions can drastically alter the resulting nuclearity and topology, highlighting the delicate balance between competitive and cooperative interactions among inorganic precursors, organophosphonates, and auxiliary solvents. The introduction of new building blocks—particularly $\{Mo_3L_2\}$ motifs—provides a structural foundation for engineering high-order architectures with tunable cavity sizes and framework rigidity. This work broadens the structural diversity of polyoxomolybdate chemistry and offers valuable insights into the rational design of gigantic POMs with controllable geometry and emerging functionalities. The introduction of functional phosphonate ligands also provides a new avenue for the development of POM clusters as promising platforms for biosensing application.

ASSOCIATED CONTENT

Supporting Information

The Supporting Information is available free of charge at https://pubs.acs.org/doi/10.1021/jacs.5c21427.

Synthetic procedure, single-crystal structure analyses, formula determination, additional structural figures, thermogravimetric analysis, UV−vis, FTIR spectra and Raman spectra, ESI-MS and NMR, as well as the solubility of compounds **1** and **5** (PDF)

Accession Codes

Deposition Numbers 2505657−2505661 contain the supplementary crystallographic data for this paper. These data can be obtained free of charge via the joint Cambridge Crystallographic Data Centre (CCDC) and Fachinformationszentrum Karlsruhe Access Structures service.

AUTHOR INFORMATION

Corresponding Authors

Weimin Xuan − *State Key Laboratory of Advanced Fiber Materials & College of Chemistry and Chemical Engineering, Donghua University, Shanghai 201620, P. R. China;* orcid.org/0000-0003-0288-1633; Email: weiminxuan@dhu.edu.cn

https://doi.org/10.1021/jacs.5c21427
J. Am. Chem. Soc. 2026, 148, 12890−12897

De-Liang Long − *School of Chemistry, University of Glasgow, Glasgow G12 8QQ, U.K.;* orcid.org/0000-0003-3241-2379; Email: deliang.long@glasgow.ac.uk

Leroy Cronin − *School of Chemistry, University of Glasgow, Glasgow G12 8QQ, U.K.;* orcid.org/0000-0001-8035-5757; Email: lee.cronin@glasgow.ac.uk

Authors

Mengyuan Cheng − *State Key Laboratory of Advanced Fiber Materials & College of Chemistry and Chemical Engineering, Donghua University, Shanghai 201620, P. R. China; School of Chemistry, University of Glasgow, Glasgow G12 8QQ, U.K.*

Yujia Li − *State Key Laboratory of Advanced Fiber Materials & College of Chemistry and Chemical Engineering, Donghua University, Shanghai 201620, P. R. China*

Rongqing Tang − *State Key Laboratory of Advanced Fiber Materials & College of Chemistry and Chemical Engineering, Donghua University, Shanghai 201620, P. R. China*

Yubin Ma − *State Key Laboratory of Advanced Fiber Materials & College of Chemistry and Chemical Engineering, Donghua University, Shanghai 201620, P. R. China*

Complete contact information is available at: https://pubs.acs.org/10.1021/jacs.5c21427

Author Contributions

The manuscript was written through contributions of all authors. All authors have given approval to the final version of the manuscript.

Notes

The authors declare no competing financial interest.

■ ACKNOWLEDGMENTS

This work was supported by the National Natural Science Foundation of China (No. 22571038, 92161111, and 21901038), the Program for Professor of Special Appointment (Eastern Scholar) at Shanghai Institutions of Higher Learning, and the Interdisciplinary Frontier Innovation Team Development Special Fund of Donghua University. We thank the staff from the College of Materials Science and Engineering (Donghua University) for X-ray data collection using Bruker D8 Venture and the staff from the BL17B1 and B18U1 beamline of the National Facility for Protein Science in Shanghai (NFPS) at the Shanghai Synchrotron Radiation Facility for assistance during data collection. We also gratefully acknowledge financial support from the EPSRC (no. EP/L023652/1; EP/R009902/1; EP/R020914/1; EP/R01308X/1; EP/S017046/1; EP/S019472/1; EP/V048341/1), the European Research Council (Project 670467 SMART-POM), and the University of Glasgow.

■ REFERENCES

(1) (a) Cronin, A. M.; Müller, A. Themed Issue: Polyoxometalate Cluster Science. *Chem. Soc. Rev.* **2012**, *41*, 7325−7648. (b) Coronado, E.; Gimenezsaiz, C.; Gomezgarcia, C. Recent Advances in Polyoxometalate-Containing Molecular Conductors. *Coord. Chem. Rev.* **2005**, *249*, 1776−1796. (c) Pope, M. T.; Müller, A. *Polyoxometalate Chemistry From Topology via Self-Assembly to Applications*; Kluwer: Dordrecht, 2002.

(2) (a) Long, D.-L.; Burkholder, E.; Cronin, L. Polyoxometalate Clusters, Nanostructures and Materials: From Self Assembly to Designer Materials and Devices. *Chem. Soc. Rev.* **2007**, *36*, 105−121. (b) Dolbecq, A.; Dumas, E.; Mayer, C. R.; Mialane, P. Hybrid Organic−Inorganic Polyoxometalate Compounds: From Structural Diversity to Applications. *Chem. Rev.* **2010**, *110*, 6009−6048. (c) Long, D.-L.; Tsunashima, R.; Cronin, L. Polyoxometalates: Building Blocks for Functional Nanoscale Systems. *Angew. Chem., Int. Ed.* **2010**, *49*, 1736−1758.

(3) (a) Wang, S.-S.; Yang, G.-Y. Recent Advances in Polyoxometalate-Catalyzed Reactions. *Chem. Rev.* **2015**, *115*, 4893−4962. (b) Liu, C.; Moussawi, M. A.; Kalandia, G.; Salazar Marcano, D. E.; Shepard, W. E.; Parac-Vogt, T. N. Cavity-Directed Synthesis of Labile Polyoxometalates for Catalysis in Confined Spaces. *Angew. Chem., Int. Ed.* **2024**, *63*, No. e202401940.

(4) (a) Xia, Y.-S.; Zhang, L.; Lu, J.-N.; Zhao, X.-H.; Dong, L.-Z.; Liu, J.; Lan, Y.-Q. A Triple Tandem Reaction for the Upcycling of Products from Poorly Selective CO_2 Photoreduction Systems. *Nat. Synth.* **2024**, *3*, 406−418. (b) Rausch, B.; Symes, M. D.; Chisholm, G.; Cronin, L. Decoupled Catalytic Hydrogen Evolution from a Molecular Metal Oxide Redox Mediator in Water Splitting. *Science* **2014**, *345*, 1326−1330.

(5) (a) Ogiwara, N.; Iwano, T.; Ito, T.; Uchida, S. Proton Conduction in Ionic Crystals Based on Polyoxometalates. *Coord. Chem. Rev.* **2022**, *462*, No. 214524. (b) Cheng, D.; Li, K.; Zang, H.; Chen, J. Recent Advances on Polyoxometalate-Based Ion-Conducting Electrolytes for Energy-Related Devices. *Energy Environ. Mater.* **2023**, *6*, No. e12341.

(6) (a) Liu, J.-C.; Zhao, J.-W.; Streb, C.; Song, Y.-F. Recent Advances on High-Nuclear Polyoxometalate Clusters. *Coord. Chem. Rev.* **2022**, *471*, No. 214734. (b) Han, Q.; He, C.; Zhao, M.; Qi, B.; Niu, J.; Duan, C. Engineering Chiral Polyoxometalate Hybrid Metal−Organic Frameworks for Asymmetric Dihydroxylation of Olefins. *J. Am. Chem. Soc.* **2013**, *135*, 10186−10189. (c) Yin, P.; Zhang, Z.-M.; Lv, H.; Li, T.; Haso, F.; Hu, L.; Zhang, B.; Bacsa, J.; Wei, Y.; Gao, Y.; et al. Chiral Recognition and Selection during the Self-Assembly Process of Protein-Mimic Macroanions. *Nat. Commun.* **2015**, *6*, No. 6475.

(7) (a) Guedes, G.; Wang, S.; Fontana, F.; Figueiredo, P.; Lindén, J.; Correia, A.; Pinto, R. J. B.; Hietala, S.; Sousa, F. L.; Santos, H. A. Dual-Crosslinked Dynamic Hydrogel Incorporating $\{Mo_{154}\}$ with pH and NIR Responsiveness for Chemo-Photothermal Therapy. *Adv. Mater.* **2021**, *33*, No. 2007761. (b) Zhang, S.; Chen, H.; Zhang, G.; Kong, X.; Yin, S.; Li, B.; Wu, L. An Ultra-Small Thermosensitive Nanocomposite with a Mo_{154}-Core as a Comprehensive Platform for NIR-Triggered Photothermal-Chemotherapy. *J. Mater. Chem. B* **2018**, *6*, 241−248.

(8) (a) Long, D.-L.; Cronin, L. Advances in Gigantic Polyoxomolybdate Chemistry. *Adv. Inorg. Chem.* **2021**, *78*, 227−267. (b) Al-Sayed, E.; Rompel, A. Lanthanides Singing the Blues: Their Fascinating Role in the Assembly of Gigantic Molybdenum Blue Wheels. *ACS Nanosci. Au* **2022**, *2*, 179−197. (c) Müller, A.; Krickemeyer, E.; Meyer, J.; Bögge, H.; Peters, F.; Plass, W.; Diemann, E.; Dillinger, S.; Nonnenbruch, F.; Randerath, M.; Menke, C. $[Mo_{154}(NO)_{14}O_{420}(OH)_{28}(H_2O)_{70}]^{(25\pm5)-}$: A Water-Soluble Big Wheel with More than 700 Atoms and a Relative Molecular Mass of About 24000. *Angew. Chem., Int. Ed.* **1995**, *34*, 2122−2124. (d) Müller, A.; Meyer, J.; Krickemeyer, E.; Diemann, E. Molybdenum Blue: A 200 Year Old Mystery Unveiled. *Angew. Chem., Int. Ed.* **1996**, *35*, 1206−1208.

(9) (a) Müller, A.; Beckmann, E.; Bögge, H.; Schmidtmann, M.; Dress, A. Inorganic Chemistry Goes Protein Size: A Mo_{368} Nano-Hedgehog Initiating Nanochemistry by Symmetry Breaking. *Angew. Chem., Int. Ed.* **2002**, *41*, 1162−1167. (b) Miras, H. N.; Cooper, G. J.; Long, D.-L.; Bögge, H.; Müller, A.; Streb, C.; Cronin, L. Unveiling the Transient Template in the Self-Assembly of a Molecular Oxide Nanowheel. *Science* **2010**, *327*, 72−74. (c) Lin, J.; Li, N.; Yang, S.; Jia, M.; Liu, J.; Li, X.-M.; An, L.; Tian, Q.; Dong, L.-Z.; Lan, Y.-Q. Self-Assembly of Giant Mo_{240} Hollow Opening Dodecahedra. *J. Am. Chem. Soc.* **2020**, *142*, 13982−13988. (d) Müller, A.; Shah, S. Q. N.; Bögge, H.; Schmidtmann, M. Molecular Growth from a Mo_{176} to a Mo_{248} Cluster. *Nature* **1999**, *397*, 48−50.

(10) (a) Müller, A.; Serain, C. Soluble Molybdenum Blues "Des Pudels Kern. *Acc. Chem. Res.* **2000**, *33*, 2−10. (b) Cheng, M.; Zhang, D.; Liu, Y.; Chen, Z.; Ma, Y.; Tang, R.; Wang, K.; Wang, H.; Long, D.-L.; Cronin, L.; Xuan, W. Breaking the Boundary of Gigantic Molybdenum Blue Clusters: From Half-Closed $\{Mo_{85}\}$ to $\{Mo_{172}\}$ Dimer. *CCS Chem.* **2025**, *7*, 2284−2292. (c) Müller, A.; Beugholt, C.; Bögge, H.; Schmidtmann, M. Influencing the Size of Giant Rings by Manipulating Their Curvatures: $Na_6[Mo_{120}O_{366}(H_2O)_{48}\text{-}H_{12}\{Pr(H_2O)_5\}_6](\sim 200H_2O)$ with Open Shell Metal Centers at the Cluster Surface. *Inorg. Chem.* **2000**, *39*, 3112−3113. (d) Bannani, F.; Floquet, S.; Leclerc-Laronze, N.; Haouas, M.; Taulelle, F.; Marrot, J.; Kögerler, P.; Cadot, E. Cubic Box versus Spheroidal Capsule Built from Defect and Intact Pentagonal Units. *J. Am. Chem. Soc.* **2012**, *134*, 19342−19345.

(11) Müller, A.; Koop, M.; Bögge, H.; Schmidtmann, M.; Beugholt, C. Exchanged Ligands on the Surface of a Giant Cluster: $[(MoO_3)_{176}(H_2O)_{63}\text{-}(CH_3OH)_{17}Hn]^{(32-n)-}$. *Chem. Commun.* **1998**, *15*, 1501−1502.

(12) Müller, A.; Krickemeyer, E.; Bögge, H.; Schmidtmann, M.; Peters, F. Organizational Forms of Matter: An Inorganic Super Fullerene and Keplerate Based on Molybdenum Oxide. *Angew. Chem., Int. Ed.* **1998**, *37*, 3359−3363.

(13) (a) Cronin, L.; Kögerler, P.; Müller, A. Controlling Growth of Novel Solid-State Materials via Discrete Molybdenum-Oxide-Based Building Blocks as Synthons. *J. Solid State Chem.* **2000**, *152*, 57−67. (b) Cronin, L.; Beugholt, C.; Müller, A. Towards the Construction of Mesoscopic Species with Emergent and Functional Properties via the Derivatisation of Molybdenum-Oxide 'Giant-Wheel' Clusters. *J. Mol. Struct.:THEOCHEM* **2000**, *500*, 181−193. (c) Cronin, L. Exploring the Hidden Constraints That Control the Self-Assembly of Nanomolecular Inorganic Clusters. *Bull. Jpn. Soc. Coord. Chem.* **2021**, *78*, 11−17.

(14) (a) Xuan, W.; Pow, R.; Zheng, Q.; Watfa, N.; Long, D.-L.; Cronin, L. Ligand-Directed Template Assembly for the Construction of Gigantic Molybdenum Blue Wheels. *Angew. Chem., Int. Ed.* **2019**, *58*, 10867−10872. (b) Duros, V.; Grizou, J.; Xuan, W.; Hosni, Z.; Long, D.-L.; Miras, H. N.; Cronin, L. Human versus Robots in the Discovery and Crystallization of Gigantic Polyoxometalates. *Angew. Chem.* **2017**, *129*, 10955−10960. (c) She, S.; Xuan, W.; Bell, N. L.; Pow, R.; Ribo, E. G.; Sinclair, Z.; Long, D.-L.; Cronin, L. Peptide Sequence Mediated Self-Assembly of Molybdenum Blue Nanowheel Superstructures. *Chem. Sci.* **2021**, *12*, 2427−2432. (d) Xuan, W.; Surman, A. J.; Miras, H. N.; Long, D.-L.; Cronin, L. Controlling the Ring Curvature, Solution Assembly, and Reactivity of Gigantic Molybdenum Blue Wheels. *J. Am. Chem. Soc.* **2014**, *136*, 14114−14120.

(15) (a) Garrido Ribó, E.; Bell, N. L.; Xuan, W.; Luo, J.; Long, D.-L.; Liu, T.; Cronin, L. Synthesis, Assembly, and Sizing of Neutral, Lanthanide Substituted Molybdenum Blue Wheels $\{Mo_{90}Ln_{10}\}$. *J. Am. Chem. Soc.* **2020**, *142*, 17508−17514. (b) Xuan, W.; Pow, R.; Watfa, N.; Zheng, Q.; Surman, A. J.; Long, D.-L.; Cronin, L. Stereoselective Assembly of Gigantic Chiral Molybdenum Blue Wheels Using Lanthanide Ions and Amino Acids. *J. Am. Chem. Soc.* **2019**, *141*, 1242−1250. (c) Felton, D. E.; Smith, K. R.; Poole, N. A.; Cronberger, K.; Burns, P. C. A New Molybdenum Blue Structure Type: How Uranium Expands This Family of Polyoxometalates. *Chem. - Eur. J.* **2024**, *30*, No. e202400678.

(16) Li, X.-X.; Li, C.-H.; Hou, M.-J.; Zhu, B.; Chen, W.-C.; Sun, C.-Y.; Yuan, Y.; Guan, W.; Qin, C.; Shao, K.-Z.; Wang, X.-L.; Su, Z.-M. Ce-Mediated Molecular Tailoring on Gigantic Polyoxometalate $\{Mo_{132}\}$ into Half-Closed $\{Ce_{11}Mo_{96}\}$ for High Proton Conduction. *Nat. Commun.* **2023**, *14*, No. 5025.

(17) Liu, J.; Jiang, N.; Lin, J.; Mei, Z.; Dong, L.; Kuang, Y.; Liu, J.; Yao, S.; Li, S.; Lan, Y. Structural Evolution of Giant Polyoxometalate: From "Keplerate" to "Lantern" Type Mo_{132} for Improved Oxidation Catalysis. *Angew. Chem., Int. Ed.* **2023**, *62*, No. e202304728.

(18) Pow, R. W.; Xuan, W.; Long, D.-L.; Bell, N. L.; Cronin, L. Embedding Alkenes within an Icosahedral Inorganic Fullerene $\{(NH_4)_{42}[Mo_{132}O_{372}(L)_{30}(H_2O)_{72}]\}$ for Trapping Volatile Organics. *Chem. Sci.* **2020**, *11*, 2388−2393.

(19) (a) Kong, H.; Ma, P.; Wang, J.; Niu, J. Overview of Organophosphonate Covalently Modified Polyoxometalates: From Synthesis, Structural Diversity to Applications. *Polyoxometalates* **2025**, *4*, No. 9140103. (b) Goura, J.; Chandrasekhar, V. Molecular Metal Phosphonates. *Chem. Rev.* **2015**, *115*, 6854−6965.

(20) (a) Cao, G.; Haushalter, R. C.; Strohmaier, K. G. A Novel Polyoxo Molybdenum (V) Organophosphonate Anion Having a Sandwich Structure: Synthesis and Crystal Structure of $[N(C_2H_5)_4]_2Na_3(H_3O)_4\{Na[Mo_6O_{15}(O_3PC_6H_5)(HO_3PC_6H_5)_3]_2\}$. Apprx. $14H_2O$. *Inorg. Chem.* **1993**, *32*, 127−128. (b) Ishaque Khan, M.; Qin, C.; Zubieta, J. Hydrothermal Synthesis and Crystal Structure of $(NH_4)_5Na_4\{Na[Mo_6O_{15}(HO_3PC_6H_5)_3(O_3PC_6H_5)]_2\}\cdot 6H_2O$. *Inorg. Chim. Acta* **1993**, *206*, 131−133. (c) Khan, M. I.; Chen, Q.; Zubieta, J. Oxomolybdenum (V) Polyanion Clusters. Hydrothermal Syntheses and Structures of $(NH_4)_5Na_4\{Na[Mo_6O_{12}(OH)_3\text{-}(O_3PC_6H_5)_4)]_2\}\cdot 6H_2O$ $(C_6H_5CH_2NMe_3)_4K_4\{K_2[Mo_6O_{12}(OH)_3\text{-}(O_3PC_6H_5)_4]_2\}\cdot 10H_2O$ and Their Relationship to the Binuclear $(Et_4N)[Mo_2O_4Cl_3(H_2O)_3]\cdot 5H_2O$. *Inorg. Chim. Acta* **1995**, *235*, 135−145. (d) Kong, H.; Liu, S.; Wang, Y.; Xu, Q.; Li, K.; Ma, P.; Wang, J.; Niu, J. Assembly of a Hexameric Cluster of Polyoxomolybdotriphosphonate Builts from $[Zn(H_2O)\{TeMo_6O_{21}\}\{N(CH_2PO_3)_3\}]^{6-}$Subunits and Its Optical and Catalytic Properties. *Inorg. Chem.* **2021**, *60*, 15759−15767.

(21) (a) Dolbecq, A.; Lisnard, L.; Mialane, P.; Marrot, J.; Bénard, M.; Rohmer, M.-M.; Sécheresse, F. Synthesis and Characterization of Octa-and Hexanuclear Polyoxomolybdate Wheels: Role of the Inorganic Template and of the Counterion. *Inorg. Chem.* **2006**, *45*, 5898−5910. (b) Nakamura, I.; Miras, H. N.; Fujiwara, A.; Fujibayashi, M.; Song, Y.-F.; Cronin, L.; Tsunashima, R. Investigating the Formation of "Molybdenum Blues" with Gel Electrophoresis and Mass Spectrometry. *J. Am. Chem. Soc.* **2015**, *137*, 6524−6530. (c) Chang, Y.-D.; Zubieta, J. Investigations into the Syntheses and Structures of Clusters of the Mo O REO_3^{2-} Systems (E= P and As). *Inorg. Chim. Acta* **1996**, *245*, 177−198. (d) Sassoye, C.; Norton, K.; Sevov, S. C. $[Mo_5^{V}Mo_7^{VI}O_{30}(BPO_4)_2(O_3P\text{-}Ph)^6]^{5-}$: A Phenyl-Substituted Molybdenum (V/VI) Boro-Phosphate Polyoxometalate. *Inorg. Chem.* **2003**, *42*, 1652−1655.

(22) Wu, S.-X.; Yang, Y.; Qin, C.; Hou, Y.-H.; Wang, X.-L.; Su, Z.-M. Organophosphate Functionalized of $\{Mo_{240}\}$ Polyoxomolybdate Dodecahedra. *Tungsten* **2023**, *5*, 247−253.

(23) (a) Xuan, W.; Pow, R.; Zheng, Q.; Watfa, N.; Long, D.-L.; Cronin, L. Ligand-Directed Template Assembly for the Construction of Gigantic Molybdenum Blue Wheels. *Angew. Chem., Int. Ed.* **2019**, *58*, 10867−10872. (b) Xuan, W.; Pow, R.; Long, D.-L.; Cronin, L. Exploring the Molecular Growth of Two Gigantic Half-Closed Polyoxometalate Clusters $\{Mo_{180}\}$ and $\{Mo_{130}Ce_6\}$. *Angew. Chem., Int. Ed.* **2017**, *56*, 9727−9731.

(24) (a) Robbins, P. J.; Surman, A. J.; Thiel, J.; Long, D.-L.; Cronin, L. Use of Ion-Mobility Mass Spectrometry (IMS-MS) to Map Polyoxometalate Keplerate Clusters and Their Supramolecular Assemblies. *Chem. Commun.* **2013**, *49*, 1909−1911. (b) Miras, H. N.; Zang, H. Y.; Long, D.-L.; Cronin, L. Direct Synthesis and Mass Spectroscopic Observation of the $\{M_{40}\}$ Polyoxothiometalate Wheel. *Eur. J. Inorg. Chem.* **2011**, *2011*, 5105−5111.

(25) Kulikov, V.; Johnson, N. A.; Surman, A. J.; Hutin, M.; Kelly, S. M.; Hezwani, M.; Long, D.-L.; Meyer, G.; Cronin, L. Spontaneous Assembly of an Organic-Inorganic Nucleic Acid Z-DNA Double-Helix Structure. *Angew. Chem., Int. Ed.* **2017**, *56*, 1141−1145.

https://doi.org/10.1021/jacs.5c21427
J. Am. Chem. Soc. 2026, 148, 12890−12897